

Dynamics of Gravity-Capillary Solitary Waves in Deep Water

ZHAN WANG¹ AND PAUL A. MILEWSKI²

¹Department of Mathematics, University of Wisconsin-Madison, Madison WI, 53706, USA

²Department of Mathematical Sciences, University of Bath, Bath, BA2 7AY, U.K.

(Received)

The dynamics of solitary gravity-capillary water waves propagating on the surface of a three-dimensional fluid domain is studied numerically. In order to accurately compute complex time dependent solutions, we simplify the full potential flow problem by taking a cubic truncation of the scaled Dirichlet-to-Neumann operator for the normal velocity on the free surface. This approximation agrees remarkably well with the full equations for the bifurcation curves, wave profiles and the dynamics of solitary waves for a two-dimensional fluid domain. Fully localised solitary waves are then computed in the three-dimensional problem and the stability and interaction of both line and localized solitary waves are investigated via numerical time integration of the equations. The solitary wave branches are indexed by their finite energy at small amplitude, and the dynamics of the solitary waves is complex involving nonlinear focussing of wave packets, quasi-elastic collisions, and the generation of propagating, spatially localised, time-periodic structures (breathers).

1. Introduction

Deep water gravity-capillary waves are relevant in a range of applications, including the understanding of the generation of waves by wind and the interpretation of satellite remote sensing data (see, for example Zhang (1995) and Wright (1978)). The study of solitary waves in this regime is of particular theoretical interest since it is *only* under the joint effects of surface tension and gravity that localised water waves in three-dimensions have been found in the water wave problem. Such localised waves have recently been observed in the experiments of Cho *et al* (2011). In the deep water limit, these Gravity-Capillary (GC) “wavepacket” solitary waves are of a fundamentally different nature from “long” solitary waves which are described approximately by the Korteweg–de Vries (KdV), Kadomtsev-Petviashvili (KP) and related equations in shallow water. The later bifurcate from linear waves at zero wavenumber whereas the former bifurcate at a finite wavenumber, and hence their oscillatory nature. These oscillatory solitary waves were seen by Ablowitz & Segur (1979) and Akylas (1993) to be approximately described by solitary wave solutions of the focussing Nonlinear Schrödinger (NLS) equation which governs the slowly varying envelope of monochromatic waves. In this regime, Akylas (1993) observed that if the phase speed (the speed of crests of the carrier wave) and the group speed (the speed of the envelope) are equal, the solitary waves of NLS will describe approximately solitary waves in the primitive fluid equations. It is simple to show that at a minimum of the phase-speed, group and phase speed coincide, and that this occurs at nonzero wavenumber in GC waves for sufficiently deep water. (The condition is that the Bond number be less than $1/3$ which roughly corresponds to a depth greater than a centimetre in the air-water problem.)

In a two dimensional fluid domain (corresponding to a one dimensional free-surface and henceforth denoted as the ‘1D problem’), wavepacket solitary waves were first computed in the full fluid equations by Longuet-Higgins (1989) and by Vanden-Broeck & Dias (1992). In three-dimensions (with a two-dimensional free-surface, denoted the ‘2D problem’), the first computations of steady solitary waves were by Părău *et al* (2005), with related work by Kim & Akylas (2005) and Milewski (2005) on reduced equations. Due to the highly oscillatory and spatially extended nature of these waves, accurate computations are challenging. Localised waves on a two-dimensional water surface are often called “lumps”, a name carried over from their shallow water counterparts which can be approximated by the localised “lump” solutions of the KP equation, but we refer to them as wavepacket solitary waves. † In this paper we focus only on the infinite depth case since for a water-air interface, any GC dynamics in water deeper than a few centimetres is essentially in the infinite depth regime. In this regime for an air-water interface, the waves bifurcate with a carrier wavelength of approximately 1.7 cm. and a speed of 23 cm./sec.

The stability and dynamics of GC solitary waves in deep water has only recently been studied. In the 1D problem, Calvo *et al* (2002) studied the question of linear stability and Milewski *et al* (2010) studied the time-dependent evolution of solitary waves (stability and collisions) in full potential flow. In 2D, there are far fewer studies. The transverse instability of line solitary waves (solitary waves of the 1D problem trivially extended in the transverse variable) has been considered by Kim & Akylas (2007) and others. Line solitary waves are unstable to transverse perturbations of sufficiently long wavelength. Fully 2D dynamics have been considered by Akers & Milewski (2010) in a one-way simplified model and in a quadratic isotropic model in Akers & Milewski (2009). The main goal of this paper is to study 2D dynamics within a close approximation of the Euler equations. A simplification that we make, suggested and used in Kim *et al* (2012) for 1D time-dependent solutions, is to take a cubic truncation of the scaled Dirichlet-to-Neuman operator that appears in the free-surface boundary conditions. (One important difference from the model of Kim *et al* (2012) is that we use the full surface tension term which results in a considerably better approximation of the full equations at larger amplitudes.) The approximation proposed is the simplest model that can *quantitatively* capture small and moderate amplitude Euler nonlinear CG solitary wave dynamics - a claim we support with 1D comparisons.

The focussing two-dimensional cubic NLS equation is central to the understanding of the existence and stability of these solitary waves. We shall see that this equation can be used to correctly predict the existence and certain instabilities of line and wave packet solitary waves, but does not capture the larger amplitude stability characteristics, the asymptotic dynamics of unstable waves nor the interaction of solitary waves. (The situation in 1D is worse, since the NLS does not even capture the instabilities of arbitrarily small waves correctly - see for example, Calvo *et al* (2002) and Milewski *et al* (2010).)

This paper is structured as follows: in Section 2 we briefly present the derivation of the cubic truncation model we shall use and discuss what can be learned about the solitary waves from the associated NLS equation. In Section 3 we present the numerical results: 1D comparisons between the cubic model and the full problem, followed by 2D bifurcation diagrams, and stability and collision calculations. In Section 4 we briefly

† Naming these waves “wavepacket” solitary waves is more appropriate since it differentiates oscillatory solitary waves bifurcating from finite wavenumber from long waves bifurcating from zero wavenumber.

introduce variations on the cubic model, principally the addition of forcing and dissipation and treating the finite depth problem.

2. Formulation

2.1. Governing Equations

Consider the three-dimensional free-surface water wave problem under the influence of both gravity and surface tension. Let (x, y) denote the horizontal plane, z the vertical direction and t time. The fluid is assumed to be inviscid and irrotational and therefore there exists a potential function ϕ , such that the fluid velocity $(u, v, w) = (\partial_x \phi, \partial_y \phi, \partial_z \phi)$. If the displacement of the water surface is designated by $z = \eta(x, y, t)$, then the governing equations for water waves read

$$\phi_{xx} + \phi_{yy} + \phi_{zz} = 0 \quad z < \eta(x, y, t) \quad (2.1)$$

$$(\phi_x, \phi_y, \phi_z) \rightarrow 0 \quad \text{as } |x| + |y| + |z| \rightarrow \infty \quad (2.2)$$

$$\eta_t + \eta_x \phi_x + \eta_y \phi_y - \phi_z = 0 \quad \text{at } z = \eta(x, y, t) \quad (2.3)$$

$$\phi_t + \frac{1}{2}[\phi_x^2 + \phi_y^2 + \phi_z^2] + g\eta = \frac{\sigma}{\rho} \nabla \cdot \left[\frac{\nabla \eta}{\sqrt{1 + |\nabla \eta|^2}} \right] \quad \text{at } z = \eta(x, y, t) \quad (2.4)$$

where $\nabla = (\partial_x, \partial_y)$ is the horizontal gradient operator, and $\nabla \cdot$ is the corresponding horizontal divergence operator. The constants g, ρ, σ are the acceleration due to gravity, density, and the coefficient of surface tension, respectively. Following Craig & Sulem (1993), who worked in the canonical variables introduced by Zakharov (1968), the Kinematic and Dynamic boundary conditions (2.3-2.4) can be recast in terms of the free surface potential $\xi(x, y, t) = \phi(x, y, \eta(x, y, t), t)$ and η as

$$\eta_t = G(\eta)\xi \quad (2.5)$$

$$\begin{aligned} \xi_t = \frac{1}{2(1 + |\nabla \eta|^2)} & \left[(G(\eta)\xi)^2 - |\nabla \xi|^2 + 2(G(\eta)\xi) \nabla \xi \cdot \nabla \eta - |\nabla \xi|^2 |\nabla \eta|^2 \right. \\ & \left. + (\nabla \xi \cdot \nabla \eta)^2 \right] - \eta + \nabla \cdot \left[\frac{\nabla \eta}{\sqrt{1 + |\nabla \eta|^2}} \right] \end{aligned} \quad (2.6)$$

$G(\eta)$ is a scaled Dirichlet to Neumann (DtN) operator yielding the vertical velocity of the free surface. It is defined by $G(\eta)\xi = \phi_z - \phi_x \eta_x - \phi_y \eta_y = \sqrt{1 + |\nabla \eta|^2} \phi_n$, where ϕ_n is the derivative of the potential in the outward normal direction to the free surface and ϕ satisfies (2.1-2.2) with $\phi(x, y, \eta(x, y, t), t) = \xi$. These equations have been also been nondimensionalized using a characteristic lengthscale $L = \left(\frac{\sigma}{\rho g}\right)^{1/2}$, a timescale $T = \left(\frac{\sigma}{\rho g^3}\right)^{1/4}$, and a resulting velocity scale $V = \left(\frac{\sigma g}{\rho}\right)^{1/4}$. In cgs units, $g = 981 \text{ cm/sec}^2$, and $\frac{\sigma}{\rho}$, the ratio of the surface tension coefficient and density, equals $73.5 \text{ cm}^3/\text{sec}^2$ for water.

2.2. Expansion and Truncation

Coifman & Meyer (1985) prove that if the L^∞ -norm and Lipschitz-norm of η is smaller than a certain constant, then G is an analytic function of η . It follows that the DtN operator can be naturally written in the form of Taylor expansion in η , $G = \sum G_i$. For

infinite depth, the first three terms of the Taylor series are given by

$$\begin{aligned} G_0 &= |D| \\ G_1(\eta) &= D \cdot \eta D - G_0 \eta G_0 \\ G_2(\eta) &= -\frac{1}{2} \left[G_0 \eta^2 |D|^2 + |D|^2 \eta^2 G_0 - 2G_0 \eta G_0 \eta G_0 \right] \end{aligned}$$

where $D = -i\nabla$ and $|D| = (-\Delta)^{1/2}$. Using the cubic truncation of G and substituted into the kinematic and dynamic boundary conditions closes the evolution problem

$$\eta_t - |D|\xi = (G_1 + G_2)\xi \quad (2.7)$$

$$\begin{aligned} \xi_t + (1 - \Delta)\eta &= \nabla \cdot \left[\frac{\nabla \eta}{\sqrt{1 + |\nabla \eta|^2}} - \nabla \eta \right] \\ &+ \frac{1}{2} \left[(G_0 \xi)(G_0 \xi - 2G_0 \eta G_0 \xi - 2\eta \Delta \xi) - |\nabla \xi|^2 \right]. \end{aligned} \quad (2.8)$$

This formulation and approximation has reduced the three dimensional nonlinear water wave problem to a two dimensional one involving only the variables on the surface that is computationally, reasonably simple. In a doubly periodic setting, each term can be efficiently computed using a pseudospectral method and the fast Fourier transform (FFT). We shall henceforth call this model the cubic Dirichelet-to-Neumann Euler equations (cDtNE). Computational methods based on series truncations of the DtN operator have been used in a variety of water wave problems and are summarised in detail by Nicholls (2007). For the 1D problem where the full equations can be numerically integrated using a conformal map method we find (see the Results section) that the cubic truncation is extremely accurate. The next physically reasonable truncation for this problem, at fifth order, would involve substantially more computational resources.

The cDtNE model can also be obtained from the fourth-order truncation of the kinetic energy part of the Hamiltonian expression of the surface water wave problem written in terms of the surface potential. The total energy of the fluid is the sum of kinetic and potential energies

$$\begin{aligned} H &= \frac{1}{2} \int dx dy \int_{-\infty}^{\eta} \left(\phi_x^2 + \phi_y^2 + \phi_z^2 \right) dz + \frac{1}{2} \int \eta^2 dx dy \\ &+ \int \left(\sqrt{1 + |\nabla \eta|^2} - 1 \right) dx dy, \end{aligned} \quad (2.9)$$

and an approximate Hamiltonian can be derived by expanding the energy in powers of the η, ξ . This takes the form

$$\begin{aligned} H[\eta, \xi] &\triangleq \tilde{H}[\eta, \xi] + O(\eta^3 \xi^2) \\ \tilde{H}[\eta, \xi] &= \int \frac{1}{2} \xi (G_0 + G_1 + G_2) \xi + \frac{1}{2} \eta^2 + \left(\sqrt{1 + |\nabla \eta|^2} - 1 \right) dx dy \end{aligned} \quad (2.10)$$

The equations (2.7) and (2.8) can be expressed in canonical form in the sense of Zakharov (1968): $\eta_t = \frac{\delta \tilde{H}}{\delta \xi}$ and $\xi_t = -\frac{\delta \tilde{H}}{\delta \eta}$. The system has further physical conserved quantities, of which mass and momentum

$$\text{Mass} = \int \eta dx dy \quad (2.11)$$

$$\text{Momentum} = \int \xi \nabla \eta dx dy, \quad (2.12)$$

are used to monitor the global accuracy of numerical computations with our truncated equations.

2.3. The Nonlinear Schrödinger Equation

Traditionally, weakly nonlinear wavepackets are studied using the resulting cubic nonlinear Schrödinger equation (NLS) for the modulational regime of monochromatic waves. It can be derived by substituting the ansatz:

$$\begin{pmatrix} \eta \\ \xi \end{pmatrix} \sim \epsilon \begin{pmatrix} A(X, Y, T) \\ B(X, Y, T) \end{pmatrix} e^{i(kx+ly-\omega t)} + c.c. + \epsilon^2 \begin{pmatrix} \eta_1 \\ \xi_1 \end{pmatrix} + \epsilon^3 \begin{pmatrix} \eta_2 \\ \xi_2 \end{pmatrix} + \dots \quad (2.13)$$

into (2.5), (2.6) and ensuring that the series is well-ordered for $t = O(\epsilon^{-2})$. Here $X = \epsilon(x - c_g t)$, $Y = \epsilon y$ and $T = \epsilon^2 t$ where c_g is the group velocity in the wave propagating direction and “c.c.” represents the complex conjugate of preceding terms. The wave envelope A can then be found to satisfy the NLS equation (Ablowitz & Segur (1979))

$$iA_T + \lambda_1 A_{XX} + \lambda_2 A_{YY} = \mu |A|^2 A \quad (2.14)$$

It is a trivial fact that substituting the same ansatz into the equations (2.7), (2.8) instead yields an NLS equation with identical coefficients - which is the motivation for choosing at least a cubic truncation of the DtN operator. We omit the details of the derivation, and just state the results. Choosing $k = 1, l = 0$ as the carrier wave, the phase and group velocity are equal, with the phase velocity at its minimum $c_{min} = \sqrt{2}$. All of the waves we consider bifurcate from this point and exist only for $c < c_{min}$. The coefficients of NLS are given by

$$\lambda_1 = \frac{\sqrt{2}}{4}, \quad \lambda_2 = \frac{\sqrt{2}}{2}, \quad \mu = -\frac{11}{8}\sqrt{2}.$$

The solution to the original system is then as follows

$$\eta = \epsilon A e^{i\Theta} - 2\epsilon^2 A^2 e^{2i\Theta} + \dots + c.c. \quad (2.15)$$

$$\xi = -i\sqrt{2}\epsilon A e^{i\Theta} + i2\sqrt{2}\epsilon^2 A^2 e^{2i\Theta} + \dots + c.c. \quad (2.16)$$

where $\Theta = x - \sqrt{2}t$. Since the NLS equation (2.14) is of the elliptic or focussing type with solitary wave solutions in both one and two dimensions, and since the phase and group speed are equal at the chosen carrier wave, one can expect small amplitude solitary waves bifurcating from a uniform flow. These solitary waves of (2.7,2.8) can be approximated by the NLS solitary waves found by solving the elliptic eigenvalue problem for $\rho(x, y)$ and Ω

$$\Delta \rho + \rho^3 = \Omega \rho, \quad \|\rho\|_\infty = 1, \quad \rho \rightarrow 0 \text{ at } \infty. \quad (2.17)$$

This is obtained by setting $A = |\mu|^{-1/2} \rho (|\lambda_1|^{-1/2} X, |\lambda_2|^{-1/2} Y) e^{-i\Omega T}$. Denoting $\Delta c \equiv \sqrt{2} - c$ where c is the wave propagating speed, then, by the chosen scaling, $\Delta c \sim \Omega \epsilon^2$. The total energy of the Gravity-Capillary solitary wave bifurcating below the minimum phase speed is then calculated by (2.10).

For the one dimensional problem (2.17) has the well known unique focussing NLS soliton, $\rho = \text{sech}(x)$, $\Omega = \frac{1}{2}$, $\int \rho^2 = 2\sqrt{2}$ and thus

$$\|\eta\|_\infty \approx \left| \frac{8}{\mu} \right|^{1/2} (\Delta c)^{1/2} + \left| \frac{8}{\mu} \right| \Delta c \quad (2.18)$$

$$\tilde{H} \approx \frac{4|\lambda_1|^{1/2}}{|\mu|} \int \rho^2 \left(\frac{\Delta c}{\Omega} \right)^{1/2} = \frac{2^{23/4}}{11} (\Delta c)^{1/2} \quad (2.19)$$

For the two dimensional case, which are the ones of interest here, there are countably

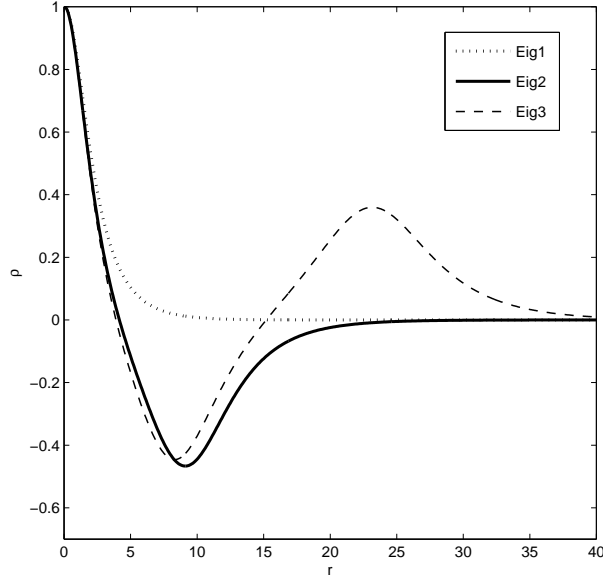


FIGURE 1. First three radially symmetric solutions of (2.17). The corresponding energies of the wavepacket solitary waves for these three envelopes are 12.04, 79.39, 201.46

many solutions to the problem (2.17) (see Alfimov *et al* (1990) and references therein), and the first three radially symmetric solutions are shown in Figure 1. For the ground state, called the Townes soliton in nonlinear optics (Chiao *et al* (1964)), $\Omega \approx 0.204$, $\int \rho^2 \approx 11.70$, and, in the present hydrodynamic context,

$$\|\eta\|_\infty \approx \left| \frac{4}{\mu\Omega} \right|^{1/2} (\Delta c)^{1/2} + \left| \frac{4}{\mu\Omega} \right| \Delta c \quad (2.20)$$

$$\tilde{H} \approx \frac{4|\lambda_1\lambda_2|^{1/2}}{|\mu|} \int \rho^2 \approx 12.04 \quad (2.21)$$

The details of these computations can be found in Akers & Milewski (2010). An interesting particularity is that the physical energy for two dimensional wavepacket solitary waves is predicted to tend to a *finite* value of 12.04 as the amplitude approaches zero, which we shall verify in the cDtNE model. This is purely a consequence of scaling: the radially symmetric envelope’s area is proportional to ϵ^{-2} exactly countering the effect of decreasing amplitude of the wave whose energy density is ϵ^2 . Shallow water lump solutions of KP (a valid approximation when the Bond number is greater than 1/3) do not have this property. The higher energy states of the eigenvalue problem (2.17) can be associated with different families of travelling waves of the cDtNE model resulting in a remarkable “quantisation” of the energy of solitary GC waves in the 2D problem.

3. Results

The numerical solution of the cDtNE system is implemented on a periodic domain with Fourier pseudo-spectral methods, where all derivatives and Hilbert transforms are computed in Fourier space with spectral accuracy, while nonlinearities are computed pseudo-spectrally in real space. For traveling waves, the resulting algebraic system for the Fourier coefficients is solved using Newton’s method using a monochromatic wave modulated by the solution to (2.17) as initial guesses. The branches are computed

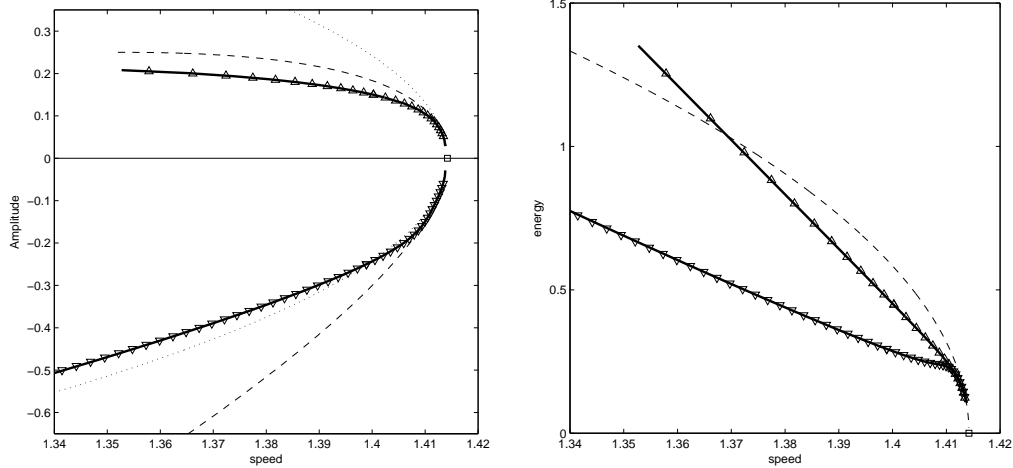


FIGURE 2. Left: 1D speed-amplitude bifurcation picture for elevation and depression solitary waves. The solid line, triangles, dotted lines and dashed lines correspond to cDtNE, Euler, leading order NLS and corrected NLS (from equation 2.19) respectively. Right: 1D speed-energy bifurcation picture for elevation and depression solitary waves. The triangles denote the Euler solutions, the solid line is the cDtNE, and the dashed line is the prediction of NLS.

through straightforward continuation methods. For time integration of the system, a classic fourth order Runge-Kutta method is used with the integrating factor method (see Milewski & Tabak (1999) for details) used to exactly integrate the linear part of the equation. The conserved quantities of the system are monitored and in all cases are preserved to a relative error of at most $O(10^{-4})$. All the computations are de-aliased with a doubling of Fourier modes. For two dimensional computations at least 256×64 modes are used along the propagating and transverse directions respectively. It is often the small amplitude solutions that are most difficult to compute accurately since the spatial decay of those solutions is much slower. Thus, the computational domain is gradually enlarged as the amplitude becomes smaller.

3.1. The 1D problem and model accuracy

The bifurcation diagrams of 1D Gravity-Capillary solitary waves for the full equations in deep water have been presented in Vanden-Broeck & Dias (1992) and others. In figure 2 we compare the speed-amplitude and speed-energy bifurcation diagrams of the cDtNE model to these and to the theoretical prediction of NLS. There, and elsewhere, we use either η at the centre of the wave or the energy \tilde{H} as the amplitude parameter. The cDtNE model agrees well with the bifurcation picture for the Euler equations far beyond the NLS regime. Typical profiles of the depression and elevation branches of waves are shown in figure 3. The model is remarkably accurate: at relatively large amplitudes which are far from the NLS regime the relative difference in profile between the full equations and the model are of order 10^{-3} and not visually discernible. Although a quantitative comparison of time-dependent dynamics is involved and beyond the scope of this paper (in particular methods used to solve the full equations usually do not use a uniform grid in x), we show an example of the inelastic overtaking collision of two solitary waves computed with the full equations (reported in Milewski *et al* (2010)) and cDtNE truncation in Figure 4. The results are extremely close and we see this as further evidence that the cDtNE model is an accurate representation of the Euler equations in a broad amplitude range of the CG regime. Comparisons that we have made with the cubic model of Kim *et al* (2012) show

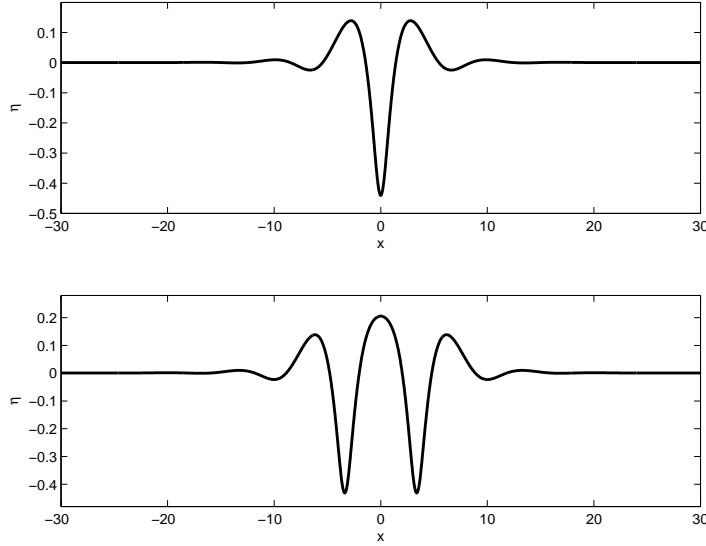


FIGURE 3. Typical free-surface solitary profiles of 1D elevation and depression solitary waves for the cDtNE model far from the NLS wavepacket regime. Top: depression wave with $\eta(0) = -0.4406$ and $c = 1.3573$. Bottom: elevation wave with $\eta(0) = 0.2055$ and $c = 1.3579$. The solution to the full equations *cannot* be visually differentiated from these on this scale. For the depression wave, the maximum difference between the cDtNE and full solutions is 6×10^{-4} .

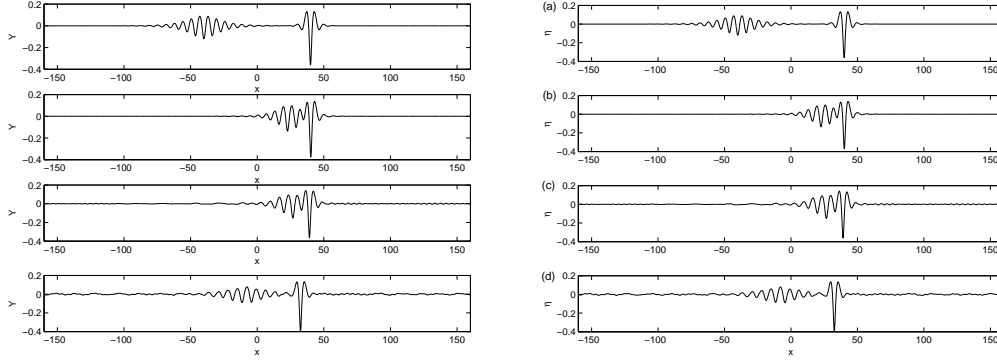


FIGURE 4. Overtaking collision of two depression waves of different amplitudes (minimum free surface heights of -0.36 and -0.12) shown in a frame of reference moving at the speed of the larger wave. From top to bottom: $t = 0$, $t = 2000$, $t = 2500$ and $t = 3500$. Only the larger wave survives the collision, with the smaller wavepacket, to the left of it eventually dispersing. Left: Full equations from Milewski *et al* (2010). Left: cDtNE

that retaining the full nonlinearity of the surface tension term is far more important than the nonlinearity associated with higher order corrections of the Dirichlet to Neumann map. One may conjecture that the surface tension term has a strong regularising effect that implies fast convergence of the DtN power series approximation throughout the evolution.

3.2. The 2D bifurcation problem

Two-dimensional GC solitary waves of the full equations in infinite depth were first computed in Părău *et al* (2005) using finite differences and boundary integral methods.

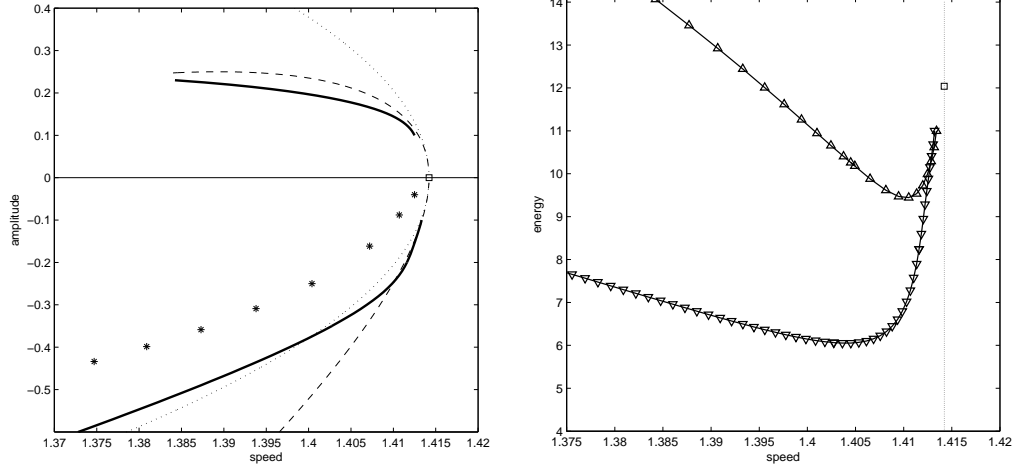


FIGURE 5. Left: Speed-amplitude bifurcation curves for elevation and depression solitary waves. The cDtNE, Euler, NLS and NLS plus correction are shown respectively by the solid, stars, dot and dash lines. Right: speed-energy bifurcation picture for both elevation (triangles pointing up) and depression (triangles pointing down). The bifurcation energy predicted by NLS is indicated by a square.

A more resolved computation was performed by Părău and reported in Cho *et al* (2011). However, this later computation is, in our opinion, also under-resolved, particularly at small amplitudes where the waves are highly oscillatory and spatially extended, as it deviates considerably from both the cDtNE and the NLS results. Figure 5 shows the bifurcation diagram of GC solitary waves, as obtained from numerical solutions of the cDtNE, full potential flow (as computed by Părău and reported in Cho *et al* (2011)), and both the leading order and leading order plus first correction of the NLS approximation. We conjecture that the cDtNE would be in quantitative agreement with full potential flow in the 2D problem given the accuracy of results at moderate amplitude in the 1D case, and the agreement with NLS approximations at small amplitude. The discrepancy between the full Euler results and the expected amplitudes predicted by NLS had been noted in Cho *et al* (2011). Furthermore, we note that the cDtNE wave packets have finite energy at their bifurcation point, as predicted by NLS but which cannot be verified in the full Euler computations at current resolution (Părău, private communication). Typical profiles of the elevation and depression waves corresponding to the bifurcation curves presented in Figure 5 are shown in Figure 6.

All solutions presented so far are those whose profile envelope at bifurcation is described by the ground state eigenfunction of (2.17). In the 2D problem, we have also computed cDtNE solitary wave solutions whose envelope is approximated by radially symmetric higher modes. For example in Figure 12 we show the unstable evolution of the complicated travelling wave resulting from the solitary wave assigned to the second radial mode of (2.17) (the wave is shown in the top-left panel of Figure 12). This wave has an energy of 79.39 at bifurcation, much higher than the ground state. Non-radially symmetric solutions to (2.17) are discussed in Alfimov *et al* (1990), but we did not attempt to compute solitary waves whose envelopes are not radially symmetric.

3.3. Stability, focussing and wave collapse

There are a few known results that guide us in a numerical study of 2D stability problem. First, it is known that both depression and elevation plane solitary waves (1D waves

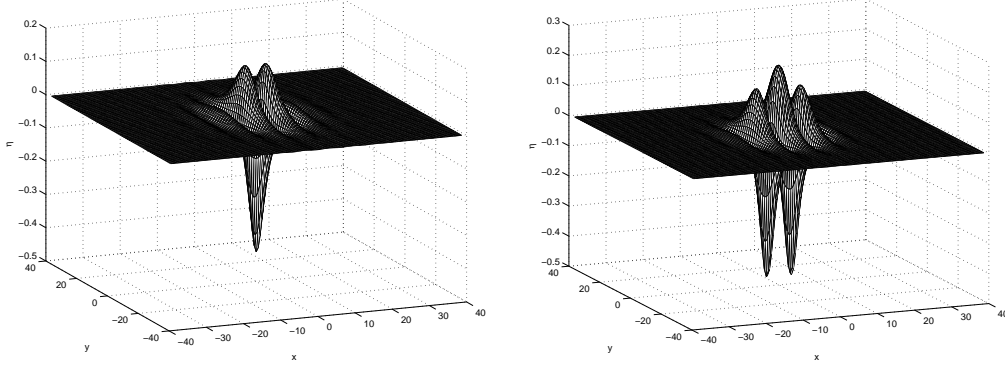


FIGURE 6. Top: representative of the depression wavepacket solitary wave solution to the cDtNE equation with $\eta(0,0) = -0.41$ and $c = 1.3907$. Bottom: representative of the elevation wavepacket solitary wave solution to the cDtNE equation with $\eta(0,0) = 0.23$ and $c = 1.3842$.

extended in the second dimension) are linearly unstable with respect to sufficiently long small perturbations in the transverse direction. This has been shown both within an NLS approximation Rypdal & Rasmussen (1988) and using arguments based on linearization of the full equations Kim & Akylas (2007). Second, in 2D the underlying focussing NLS equation (2.14) is well known to exhibit a finite-time focussing blowup called wave collapse when, in an unbounded setting, the initial conserved energy $E = \int |\nabla A|^2 - \frac{1}{2}|A|^4$, is negative (see Zakharov (1972) and Sulem & Sulem (1999)). (Note that this energy is not the same one arising from the cDtNE equations.) The result is obtained by a virial argument, whence $M_0 = \int |A|^2$ is conserved and $M_2(t) = \int (X^2 + Y^2)|A|^2$ satisfies $M'' = 8E$. Solitary waves which are solutions to the eigenvalue problem (2.17) are critical with $E = 0$. Thus, a small negative energy perturbation leads to focussing and blowup and a positive energy perturbation leads to spreading of the underlying wave envelope. We thus expect, and will confirm numerically, the instability of localised solitary wave solutions for nonzero envelope energy perturbations in the near-NLS limit of the cDtNE model (where solitary wave envelopes are well approximated by the NLS). We note that the simple virial argument is not available in a periodic setting (see Sulem & Sulem (1999)) but nevertheless seems to predict stability very well in our computations on periodic domains. Third, both elevation and depression wave branches have critical point in their speed-energy relation (see Figure 5), which can lead to an exchange of linear stability of the eigenfunction of the linearized problem associated to the translational invariance symmetry (see, for example, Akylas & Cho (2008)). This is the instability commonly observed in small amplitude elevation waves of the 1D problem leading to the eventual development of a depression wave Milewski *et al* (2010).

All figures of solitary wave dynamics presented are shown in a frame moving with the speed of the wave that was used to construct the initial data. In this frame the main features of the wave evolve slowly.

For plane solitary waves, the linear analysis based on NLS (see Akers & Milewski (2010)) shows that the transverse perturbation e^{ily} is unstable, when the wave number l in the y direction satisfies

$$|l| \lesssim \left| \frac{3\mu}{8\lambda_2} \right|^{1/2} \|u\|_\infty \approx (18)^{1/4} (\Delta c)^{1/2} \triangleq l_c \quad (3.1)$$

We confirm this in our numerical experiments where a plane solitary wave is perturbed

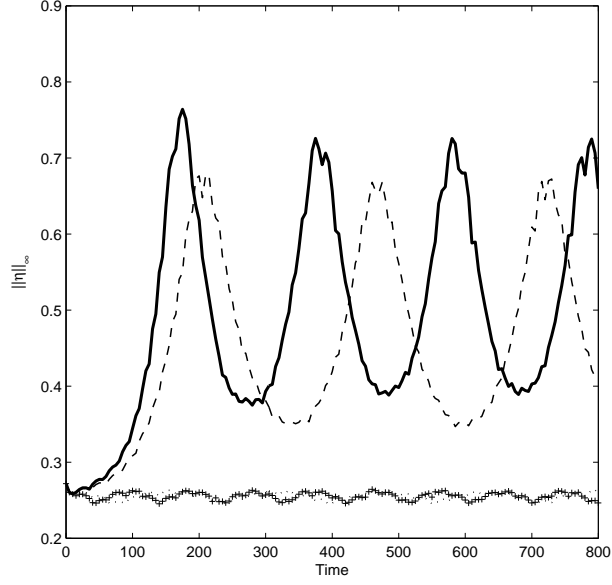


FIGURE 7. Transversal instability of the plane solitary wave, $c = 1.3994$, $\eta(0) = -0.247$. The transverse perturbation is obtained by taking an initial data of the form $\eta(x, y, 0) = [1 + 0.1 \cos(al_c y)]\tilde{\eta}(x)$, where $\tilde{\eta}(x)$ is a travelling wave solution in 1D, $l_c = 18^{1/4} \Delta c^{1/2}$, and $a = 0.8$ (solid line), $a = 0.9$ (dashed line), $a = 1.1$ (dotted line), $a = 1.2$ (plus line)

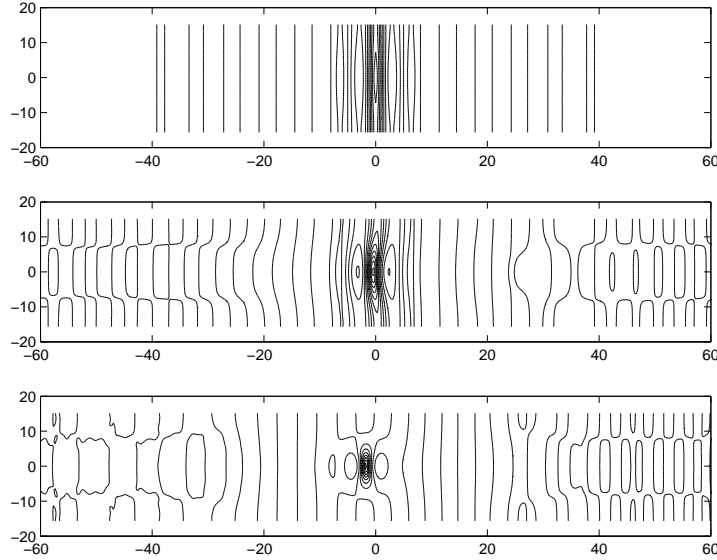


FIGURE 8. Evolution of the transverse instability to a localised solution in the case of $a = 0.8$ in Figure 7. The contours are shown from top to bottom at $t = 0$, $t = 125$, $t = 175$.

with four transverse perturbations of different wavelengths and the subsequent nonlinear evolution is compared. The perturbation wavenumbers are $l = 1.2l_c, 1.1l_c, 0.9l_c$, and $0.8l_c$ respectively. As shown in Figure 7 the first two perturbations do not destabilise the plane wave whereas the next two do. The subsequent evolution of the instability shows a focussing behaviour reminiscent of the underlying collapse dynamics of NLS as

shown in Figure 8. This intermediate time focussing is arrested by the generation of a travelling *breather*: a propagating periodic-in-time localised structure. This structure is best described as a localised depression solitary wave with periodic amplitude modulation, and which appears to be stable (see evolution for $t > 175$ in Figure 7) in all our experiments. These breathers are very common and also occur in the nonlinear evolution of instabilities of small amplitude fully localised solitary waves below.

Throughout our computations in this section, instabilities and wave interactions will invariably lead to some high frequency dispersive radiation and thus, due to our use of a periodic domain, the remaining coherent structures are embedded in a “sea” of linear ripples. This is visible in most computations and can also be seen as further evidence of the stability of the resulting structures.

The stability of localised traveling waves is considered next. First, the virial argument sketched above implies that near the bifurcation point, both elevation and depression solitary waves are linearly unstable. The virial argument would predict eventual blowup for negative energy perturbations and this is not observed, in all cases the blowup is arrested by the generation of a larger amplitude breather. Dispersive spreading consistent with the envelope spreading predicted by the virial argument is observed for positive energy perturbations. In the computations that we present we perturb the exact solitary wave solution by a small multiple of itself, by taking initial data $\eta(x, y, 0) = (1 + \delta)\tilde{\eta}$ where $\tilde{\eta}$ is the computed travelling wave. Since, for the perturbed wave,

$$E = \int |\nabla A|^2 - \frac{1}{2}|A|^4 \approx -\delta \int |\tilde{A}|^4,$$

where \tilde{A} is the envelope of the solitary wave, negative energy perturbations correspond to $\delta > 0$ and positive energy ones to $\delta < 0$. In the left panel of Figure 9 we show the typical evolution of the amplitude for a perturbed small amplitude depression solitary wave. For a negative energy perturbation we see focussing arrested by the formation of a breather whereas for positive energy the amplitude decreases monotonically as a result of dispersive spreading. The case shown is for a depression wave, however the elevation wave dynamics is broadly similar. In Figure 10 we show four snapshots of the breather evolution resulting from the unstable small amplitude depression wave at later times.

For a large class of problems, linear stability may change at a critical point of $H(c)$, the speed-energy curve. This necessary condition for instability was observed by Saffman (1985), for gravity waves and has since been extended to many other situations. Akylas & Cho (2008) present an application of this result to a wavepacket solitary wave in a model equation. In the present problem, both depression and elevation waves have critical points in $H(c)$. We denote solitary waves with speed lower than this critical speed “large amplitude” and those with speed larger than it “small amplitude” since in all our computations amplitude is a monotonic function of speed. Small amplitude waves’ bifurcation diagram and linear stability are well described by the NLS equation whereas large amplitude waves’ are not. Our numerical simulations show that for depression waves, the exchange of stability does take place at the minimum point in $H(c)$. The evolution of large amplitude depression waves’ amplitudes when subject to perturbations is shown in the right panel of Figure 9. The waves are stable regardless of the sign of δ . Solitary waves (or breathers which are small perturbations of the solitary waves) propagate in the midst of small linear dispersive waves that have been shed by the perturbed initial data.

All our computations show that elevation waves remain unstable at large amplitude. In Figure 11 an unstable large elevation solitary wave subject to a small negative energy perturbation and evolves into a depression breather. Similarly, positive energy perturbations will also yield depression breathers (whose energy is much smaller than the elevation

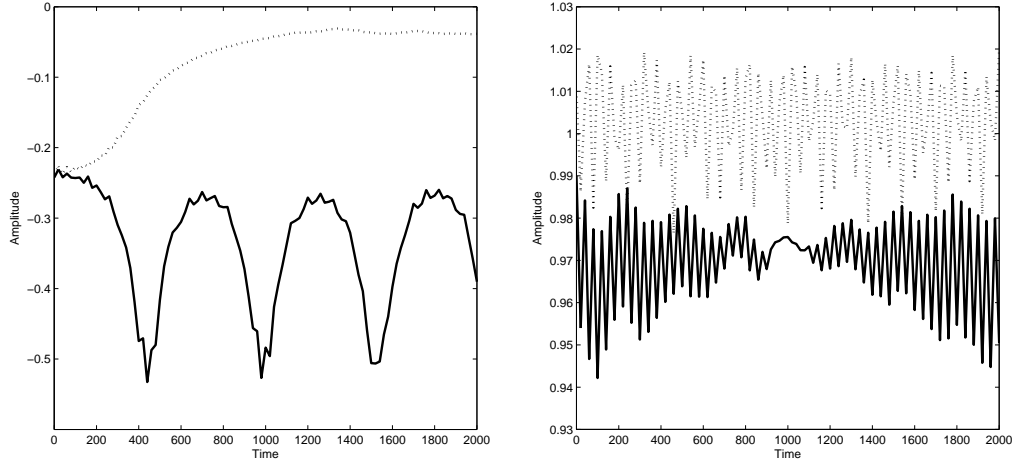


FIGURE 9. Left: evolution of maximum trough depth for perturbed depression waves in the small amplitude regime ($\eta(0,0) = -0.24$ and $c = 1.4103$). Negative energy perturbation ($\delta = 0.01$) is shown by a solid line, and positive energy ($\delta = -0.01$) by a dashed line. Right: evolution of maximum trough depth (normalised by initial maximum trough depth) for depression waves in the large amplitude regime ($\eta(0,0) = -0.49$ and $c = 1.3873$). Positive energy perturbation ($\delta = 0.01$) is shown by a solid line, and negative energy ($\delta = -0.01$) by a dashed line.

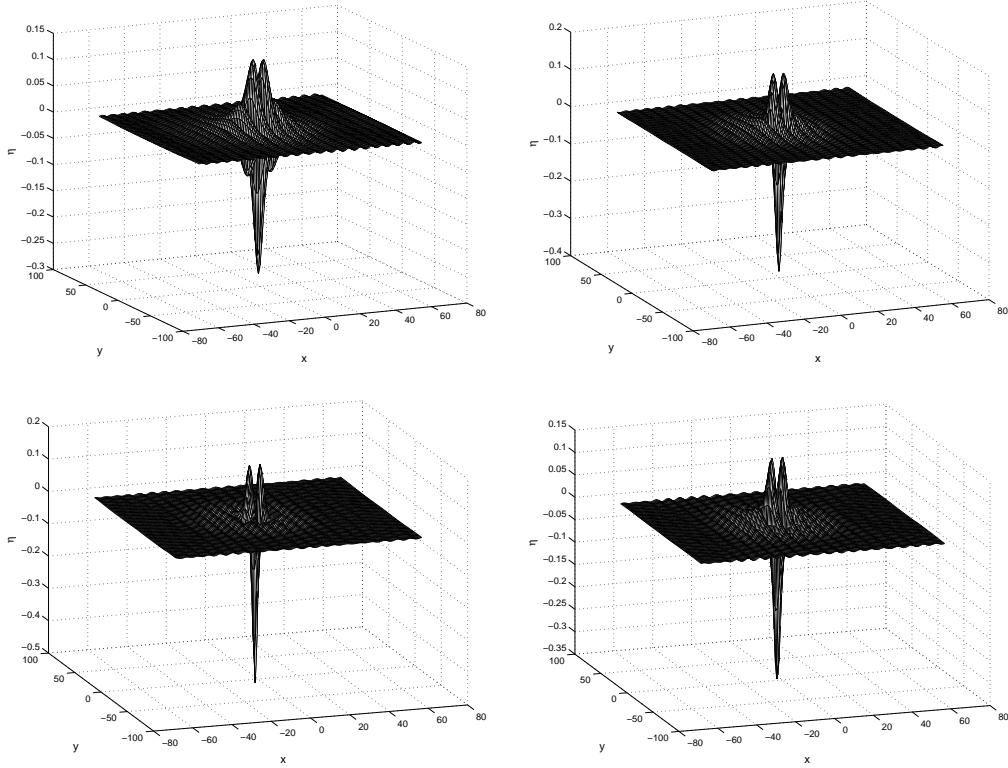


FIGURE 10. From top-left to bottom-right: snapshots of one period of a breather taken at $t = 1240, 1440, 1520, 1620$ for the small amplitude negative energy computation discussed in Figure 9.

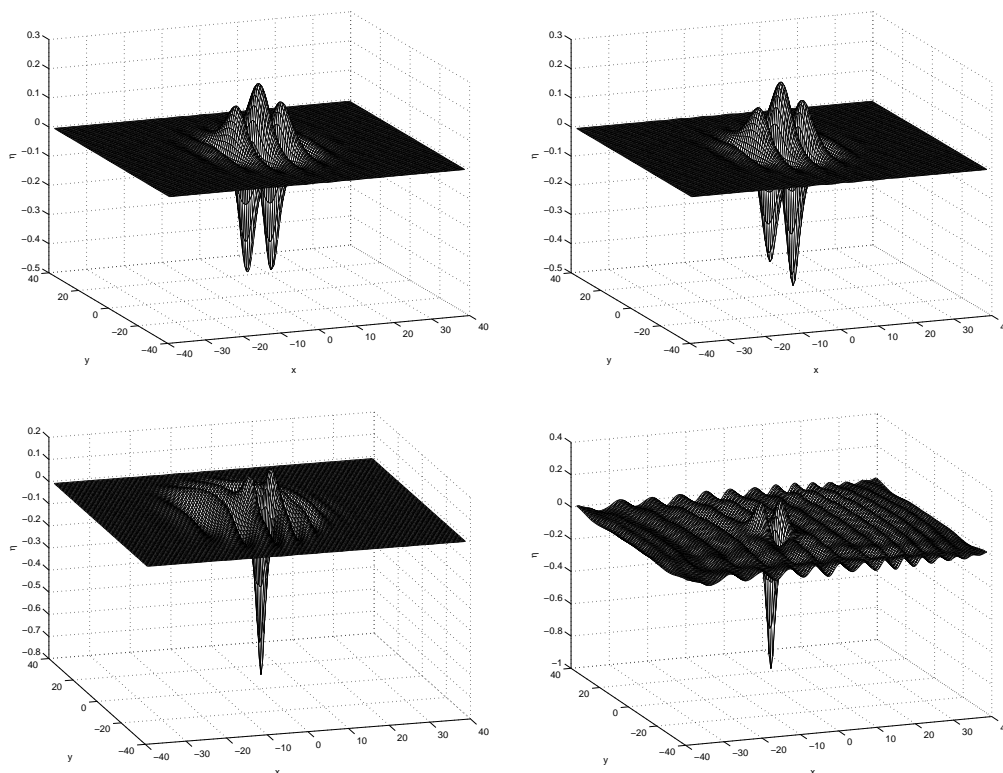


FIGURE 11. From top-left to bottom-right: snapshots of the evolution of a large amplitude unstable elevation wave with $\eta(0,0) = 0.2196$, $c = 1.3907$ in cDtNE at $t = 0, 120, 200, 270$. The perturbation is 0.01 times the original solitary wave. Some waves are radiated during the transition and the unstable wave evolves into a breather.

waves (see Figure 5). The instability is initially similar to that of a 1D depression wave (see Milewski *et al* (2010)): a symmetry breaking whereby the leading trough grows at the expense of the trailing one (this instability is associated to the translational invariance mentioned above). What follows is collapse focussing that is arrested by the formation of a depression breather.

From our calculations, we believe there are families of periodic (breather) solutions of different periods and amplitude for each fixed energy above the minimum of the depression solitary waves. The orbits of these breathers in phase space are centred around the fixed point of stable depression solitary waves and the precise bifurcation diagram for them would require computing exact periodic localised structures which is beyond the scope of this paper. A summary of the stability results in this section is shown in table 3.3.

Lastly we compute the evolution of a complex solitary wave of the cDtNE equations corresponding to a higher mode of the nonlinear eigenvalue problem discussed previously, and this is shown in Figure 12. In this case all perturbations triggered rapid instabilities, but the nonlinear evolution shows a remarkable dynamics with eventual focussing into four depression breathers of different amplitudes.

3.4. Collisions

Given the stability of large amplitude depression waves, we have numerically computed their collisions. We have only computed head-on and overtaking collisions of pairs of

	positive energy perturbation	negative energy perturbation
small depression	unstable→large breather	unstable→disperses out
small elevation	unstable→large breather	unstable→disperses out
large depression	stable	stable
large elevation	unstable→large breather	unstable→large breather

TABLE 1. Summary of stability Results

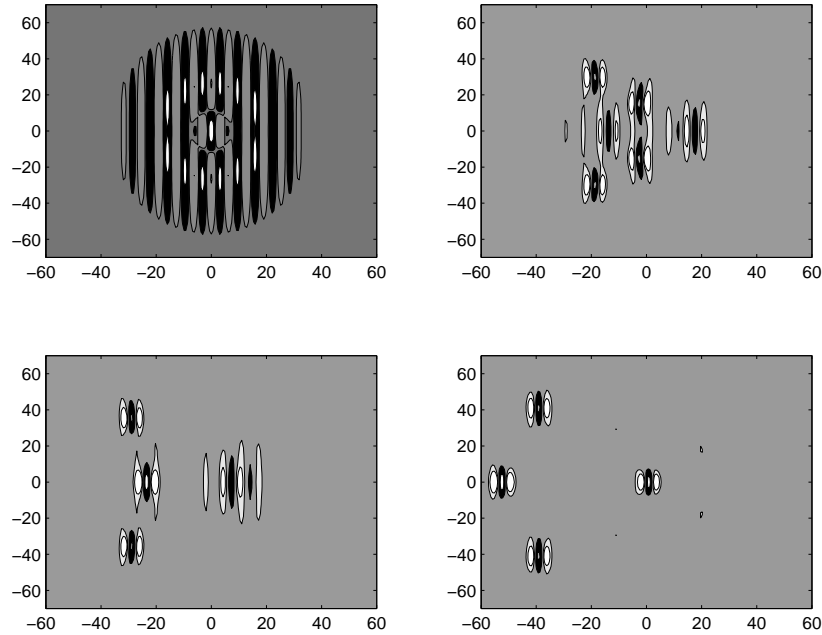


FIGURE 12. Instability of a higher energy solitary wave with $\eta(0,0) = -0.4028, c = 1.4061$. Snapshots of the evolution are shown at $t = 0$ (top left), $t = 800$ (top right), $t = 1200$ (bottom left), $t = 1600$ (bottom right). Four depression breathers emerge from the complex behaviour.

waves although in a 2D problem there is a wide range of possible collision scenarios. For head-on collisions, the interaction time between the two waves is insufficient for any strong nonlinear effect to take place and we have only observed very small oscillations that result from the small inelasticity of the collision. The waves essentially traverse each other. The more interesting case is the overtaking collision. Here, the small difference in solitary wave speeds implies that the calculations must be carried out over long times. In the 1D problem collisions were of two types of inelastic collisions Milewski *et al* (2010): collisions where both waves survived and collisions where only the larger wave survived when their amplitude difference was large. Here, we have only observed quasi-elastic collisions where both waves survive and the primary effect of the overtaking collision is a rapid and large phase shift of the order of one envelope wavelength. Figure 13 shows the before and after free surface profiles of the waves and Figure 14 shows the resulting waves' trajectories in (x, t) space. The collisions are weakly inelastic and the wave amplitude is mildly attenuated with some dispersive radiation present during the collision.

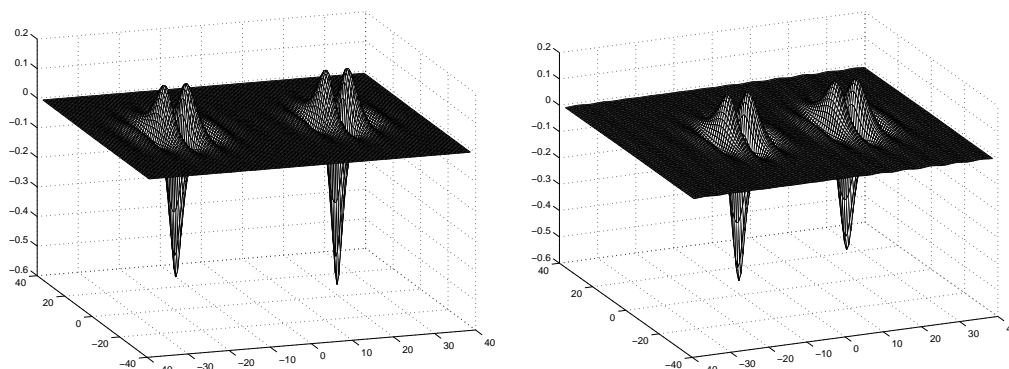


FIGURE 13. Collision of two stable depression solitary waves travelling in the positive x -direction. Left: Initial data consisting of a shifted superposition of two waves with $\eta(0,0) = -0.56$, $c = 1.3782$ and $\eta(0,0) = -0.49$, $c = 1.3873$. Right: Solution after interaction at $t = 4000$. Note that the collision is not completely elastic, with their amplitudes decreasing slightly as a result of the collision. The solution was computed in a frame of reference moving at speed 1.3828.

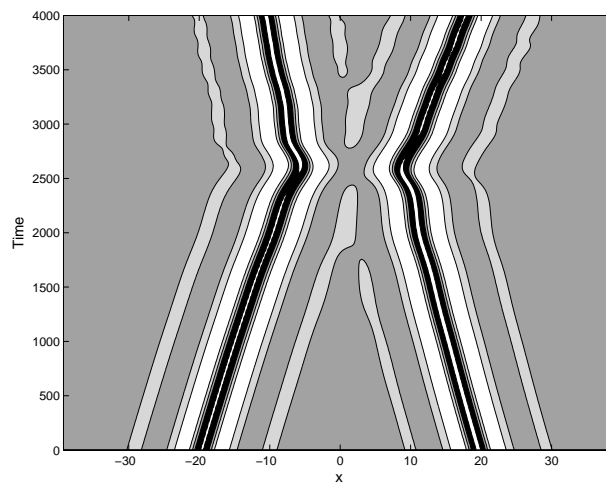


FIGURE 14. Filled contour plot of the centreline of the dynamics $\eta(x,0,t)$ for the collision reported in Figure 13. Note that the waves' core remain distant during the collision and that after the collision the waves have exchanged identities and undergone a phase shift.

4. Extensions

There are several extensions of the model which, while the detailed study is beyond the scope of this paper, may be useful in studying problems of this type. We have considered fluids of infinite depth only (which in the case of GC flows in water is a good approximation for depths exceeding a few centimetres). If the effect of finite depth is required, the formulation can be modified simply by taking $G_0(\eta) = |D| \tanh(h|D|)$ where h is the mean depth of the fluid normalised by the capillary gravity length scale and is inversely related to the Bond number. In particular the shallow water lump dynamics modelled by the Kadomtsev-Petviashvili (KP) equation should be recovered when the Bond number is greater than $1/3$.

Given the small length scales of the waves, it may also be of practical interest to add the effects of viscosity and forcing. In the analysis of their experiments Cho *et al* (2011)

adjusted a simple one-way model proposed in Akers & Milewski (2009) by adding forcing and a viscous damping. The more accurate cDtNE equations can be modified to include small viscous damping effects by using the approximation presented in Dias *et al* (2008) whereby dissipation is modelled through the modification of both kinematic and dynamic boundary conditions:

$$\eta_t - G_0\xi = 2Re^{-1}\Delta\eta + (G_1 + G_2)\xi \quad (4.1)$$

$$\begin{aligned} \xi_t + (1 - \Delta)\eta = 2Re^{-1}\Delta\xi + P(x, y, t) + \nabla \cdot \left[\frac{\nabla\eta}{\sqrt{1 + |\nabla\eta|^2}} - \nabla\eta \right] \\ + \frac{1}{2} \left[(G_0\xi)(G_0\xi - 2G_0\eta G_0\xi - 2\eta\Delta\xi) - |\nabla\xi|^2 \right]. \end{aligned} \quad (4.2)$$

Here, $P(x, y, t)$ is the pressure forcing and the Reynolds number, which controls the dissipation rate, is given by

$$Re = \frac{VL}{\nu} = \frac{(\sigma/\rho)^{3/4}}{g^{1/4}\nu},$$

where ν is the kinematic viscosity of the fluid. For the case of an air-water interface in the regime that we considered in this paper, we obtain a Reynolds number of approximately 500.

For small amplitude waves, the variation in the transverse direction is not significant compared to that in the propagation direction. One can therefore propose to assume this a priori and simplify the system by deleting all the nonlinear terms which include y -derivatives obtaining a “weakly transversal” model which still has the same NLS equation describing wave packets as the full problem. The Hamiltonian for this model reads

$$\overline{H}[\eta, \xi] = \int \frac{1}{2}\xi(G_0 + \overline{G}_1 + \overline{G}_2)\xi + \frac{1}{2}\eta^2 + \frac{1}{2}\eta_y^2 + (\sqrt{1 + \eta_x^2}) dx dy \quad (4.3)$$

where

$$\begin{aligned} \overline{G}_0 &= (-\partial_{xx})^{1/2} \\ \overline{G}_1 &= -\partial_x\eta\partial_x - \overline{G}_0\eta\overline{G}_0 \\ \overline{G}_2 &= \frac{1}{2}\overline{G}_0\eta^2\partial_{xx} + \frac{1}{2}\partial_{xx}\eta^2\overline{G}_0 + \overline{G}_0\eta\overline{G}_0\eta\overline{G}_0 \end{aligned} \quad (4.4)$$

Calculations performed with this approximation show excellent agreement with cDtNE at small amplitudes and only qualitative agreement for larger amplitude solitary waves.

5. Conclusions

The dynamics of Gravity-Capillary solitary waves on the surface of three-dimensional fluid was studied. The only approximation made was a cubic truncation of a scaled Dirichlet to Neumann map that provides the normal velocity of the free-surface given its tangential velocity. In two dimensions, where comparisons to the untruncated problem (i.e. fully nonlinear free-surface potential flow) can be accurately measured, this truncation is remarkably accurate in modelling small and moderate amplitude waves. We conjecture that the same is true in three-dimensions.

There are undoubtedly in this problem infinitely many branches of solitary travelling wave solutions as this is the prediction of the associated envelope NLS analysis about the bifurcation point. We compute examples of three of them: elevation and depression solitary waves arising from the simplest eigenfunction of the NLS problem and a more complex wave arising from a higher eigenfunction of the same problem. The localised

solitary waves have the surprising property that as their amplitude (from peak to trough) decreases to zero as the bifurcation point is approached, their physical energy tends to a finite positive value, quantised by the different eigenfunctions of the NLS equation.

The instability and subsequent evolution for one dimensional line solitary waves and the various two dimensional solitary waves have been explored numerically by perturbing the waves and computing the solution through accurate pseudo spectral based methods. All solitary waves are found to be unstable with the notable exception of larger amplitude depression waves. These waves together with travelling breathers, which are periodic travelling cycles oscillating about these travelling states, are stable and appear to be attractors in the long time evolution of the problem.

The focussing NLS equation adequately predicts the bifurcation and linear stability properties of small amplitude solitary CG waves. The collapse singularity of initial data, however, is not observed in our computations leading to the conjecture that an appropriate envelope model for this problem is a cubic-quintic NLS equation where the quintic term is defocussing.

Acknowledgements

We thank Dr E. Părău for making available more resolved numerical results solitary waves. This work was supported by EPSRC, under Grant Number GR/S47786/01, by the Division of Mathematical Sciences of the National Science Foundation, under Grant Number DMS-0908077, and by a Royal Society Wolfson award.

REFERENCES

- ABLOWITZ, M. J. & SEGUR, H. (1979) On the evolution of packets of water waves. *J. Fluid Mech.* **92**, 691-715.
- ALFIMOV, G. L., ELEONSKY, V. M., KULAGIN, N. E., LERMAN, L. M. & SILIN, V. P. (1990) On existence of nontrivial solutions for the equation $\Delta u - u + u^3 = 0$. *Physica D* **44**, 168-177.
- AKERS, B. & MILEWSKI, P. A. (2010) Dynamics of three-dimensional gravity-capillary solitary waves in deep water. *SIAM J. Appl. Math.* **70**, 2390-2408.
- AKERS, B. & MILEWSKI, P. A. (2009) A model equation for wavepacket solitary waves arising from capillary-gravity flows. *Stud. in Appl. Math.* **122**, 249-274.
- AKYLAS, T. R. (1993) Envelope solitons with stationary crests. *Phys. Fluids A* **5**, 789-791.
- AKYLAS, T. R. & CHO, Y. (2008) On the stability of lumps and wave collapse in water waves. *Phil. Trans. Math. Phys. Eng. Sci.* **366**, 2761-2774.
- CHIAO, R. Y., GARMIRE, E. & TOWNES, C. (1964) Self-trapping of optical beams. *Phys. Rev. Lett.* **13**, 479-482.
- CHO, Y., DIORIO, J. D., DUNCAN, J. H. & AKYLAS, T. R. (2011) Resonantly forced gravity-capillary lumps on deep water. Part 1. Experiments. *J. Fluid Mech.* **672**, 268-387.
- CHO, Y., DIORIO, J. D., AKYLAS, T. R. & DUNCAN, J. H. (2011) Resonantly forced gravity-capillary lumps on deep water. Part 2. Theoretical model. *J. Fluid Mech.* **672**, 288-306.
- COIFMAN, R. & MEYER, Y. (1985) Nonlinear harmonic analysis and analytic dependence. *Proc. Symp. Pure Math.* **43**, 71-78.
- CRAIG, W. & SULEM, C. (1993) Numerical simulation of gravity waves. *J. Comp. Phys.* **108**, 73-83.
- CALVO, D. C., YANG, T. S. & AKYLAS, T. R. (2002) Stability of steep gravity-capillary waves in deep water. *J. Fluid Mech.* **452**, 123-143.
- DIAS, F., DYACHENKO, A. I. & ZAKHAROV, V. E. (2008) Theory of weakly damped free-surface flow: A new formulation based on potential flow solutions. *Phys. Lett. A* **372**, 1297-1302.
- IOOSS, G. & KIRRMANN, P. (1996) Capillary gravity waves on the free surface of an inviscid fluid of infinite depth-Existence of solitary waves. *Arch. Rat. Mech. Anal.* **136**, 1-19.
- KIM, B. & AKYLAS, T. R. (2005) On gravity-capillary lumps. *J. Fluid Mech.* **540**, 337-351.

- KIM, B. & AKYLAS, T. R. (2007) Transverse instability of gravity-capillary solitary waves. *J. Eng. Math.* **58**, 167-175.
- KIM, B., DIAS, F. & MILEWSKI, P. A. (2012) On weakly nonlinear gravity-capillary solitary waves. Part 1. Bifurcation of solitary wavepackets. *Wave Motion* **49**(2), 221-237.
- LONGUET-HIGGINS, M. S. (1989) Capillary-gravity waves of solitary type on deep water. *J. Fluid Mech.* **200**, 451-478.
- MILEWSKI, P. A. (2005) Fast communication: Three-dimensional localized gravity-capillary waves. *Comm. Math. Sci.* **3**, 89-99.
- MILEWSKI, P. A. & TABAK, E. G. (1999) A pseudospectral procedure for the solution of nonlinear wave equations with examples from free-surface flows. *SIAM J. Sci. Comput.* **21**(3), 1102-1114.
- MILEWSKI, P. A., VANDEN-BROECK, J.-M. & WANG, Z. (2010) Dynamics of steep two-dimensional gravity-capillary solitary waves. *J. Fluid Mech.* **664**, 466-477.
- NICHOLLS, D. P. (2007) Boundary perturbation method for water wave. *GAMM-Mitt* **30**(1), 44-74.
- PĂRĂU, E. I., VANDEN BROECK, J.-M. & COOKER, M. J. (2005) Nonlinear three-dimensional gravity-capillary solitary wave. *J. Fluid Mech.* **536**, 99-105.
- RYPDAL, K. & RASMUSSEN, J. J. (1988) Stability of solitary structures in the nonlinear Schrödinger equations, *Physica Scripta* **40**, 192-201.
- SAFFMAN, P. G. (1985) The superharmonic instability of finite amplitude water waves. *J. Fluid Mech.* **159**, 169-174.
- SULEM, C. & SULEM, P. L. (1999) *The nonlinear Schrödinger equation: self-focusing and wave collapse*, Applied Mathematical Sciences 139, Springer.
- VANDEN-BROECK, J.-M. & DIAS, F. (1992) Gravity-capillary solitary waves in water of infinite depth and related free-surface flows. *J. Fluid Mech.* **240**, 549-557.
- WRIGHT, J. W. (1978) Detection of ocean waves by microwave radar: the modulation of short gravity-capillary waves. *Boundary Layer Meteorology* **13**, 87-105.
- ZAKHAROV, V. E. (1968) Stability of periodic waves of finite amplitude on the surface of a deep fluid. *J. Appl. Mech. Tech. Phys.* **2**, 190-194.
- ZAKHAROV, V. E. (1972) Collapse of Langmuir waves. *Sovi. Phys. JETP* **35**(5), 908-914.
- ZHANG, X. (1995) Capillary-gravity and capillary waves generated in a wind wave tank: Observations and theory. *J. Fluid Mech.* **289**, 51-82.